Spray Dried Rugose Lipid Particle Platform for Respiratory Drug Delivery

Hui Wang[1], Mani Ordoubadi[1], Patrick Connaughton[2], Kellisa Lachacz[2], Nicholas Carrigy[2], Scott Tavernini[1], Andrew R. Martin[1], Warren H. Finlay[1], David Lechuga-Ballesteros[2], Reinhard Vehring[1]

[1] Department of Mechanical Engineering, University of Alberta, Alberta, Canada

[2] Inhalation Product Development, Pharmaceutical Technology & Development, Operations, AstraZeneca, South San Francisco, CA, USA

ABSTRACT

Purpose

To develop a new lipid-based particle formulation platform for respiratory drug delivery applications. To find processing conditions for high surface rugosity and manufacturability. To assess the applicability of the new formulation method to different lipids.

Methods

A new spray drying method with a simplified aqueous suspension feedstock preparation process was developed for the manufacture of rugose lipid particles of 1,2-distearoyl-sn-glycero-3-phosphocholine (DSPC). A study covering a wide range of feedstock temperatures and outlet temperatures was conducted to optimize the processing conditions. Aerosol performance was characterized *in vitro* and *in silico* to assess the feasibility of their use in respiratory drug delivery applications. The applicability of the new spray drying method to longer-chain phospholipids with adjusted spray drying temperatures was also evaluated.

Results

Highly rugose DSPC lipid particles were produced via spray drying with good manufacturability. A feedstock temperature close to, and an outlet temperature lower than, the main phase transition were identified as critical in producing particles with highly rugose surface features. High emitted dose and total lung dose showed promising aerosol performance of the produced particles for use as a drug loading platform for respiratory drug delivery. Two types of longer-chain lipid particles with higher main phase transition temperatures, 1,2-diarachidoyl-sn-glycero-3-phosphocholine (DAPC) and 1,2-dibehenoyl-sn-glycero-3-phosphocholine (22:0 PC), yielded similar rugose morphologies when spray dried at correspondingly higher processing temperatures.

Conclusions

Rugose lipid particles produced via spray drying from an aqueous suspension feedstock are promising as a formulation platform for respiratory drug delivery applications. The new technique can potentially produce rugose particles using various other lipids.

KEYWORDS

Spray drying; rugose lipid particle; particle engineering; respiratory drug delivery; formulation platform.

INTRODUCTION

Inhalation therapy has long been proven the most efficacious route of drug administration in the treatment of airway diseases such as asthma, cystic fibrosis, and chronic obstructive pulmonary disease (COPD). The past decades have seen an emerging interest in the use of the respiratory route for the systemic administration of various drugs and biopharmaceuticals to treat non-pulmonary diseases as well (1). Despite the long history of delivering medication through inhalation (2), limited types of inhalation delivery systems are available, with the three main categories being nebulizers, pressurized metered-dose inhalers (pMDIs), and dry powder inhalers (DPIs) (3).

Different inhaled drug delivery devices produce respirable aerosols via different mechanisms. Nebulizers are available in various forms based on the nebulization mechanism used; they include jet nebulizers, ultrasonic nebulizers, and vibrating mesh nebulizers. These all serve to aerosolize drug solutions and sometimes suspensions into liquid droplets in the respirable range (1 – 5 μm), which are then continuously delivered to patients for inhalation for an extended period to achieve a targeted dose (4). Low drug delivery efficiency, poor patient compliance, and lengthy administration time have been identified as some of the challenging aspects of nebulized therapy (4). As the most widely used inhalers for respiratory drug delivery, pressurized metered-dose inhalers contain active pharmaceutical ingredients suspended or dissolved in a pressurized liquid. Upon actuation, a metered dose of the drug suspension or solution is released as a burst of fast-evaporating droplets, leaving dried respirable particles to be inhaled by the patients (5, 6). Most dry powder inhalers contain micronized cohesive drug particles blended with coarse carrier particles to improve the powder flowability (7). During inhalation, the drug particles are detached from the surface of the carrier particles by the inspiratory flow, resulting in the impaction of larger carrier particles in the upper airways and penetration of finer drug particles to the deep lung (8). Dry powder inhalers are deemed cost-effective, environmentally friendly, and easy-to-use devices that require minimum patient coordination between breathing and actuation of the device (3, 9).

Many active pharmaceutical ingredients are by themselves not suitable for direct respiratory delivery because they are too cohesive in micronized or spray-dried form. One critical aspect of inhalation formulation development, especially for DPIs, requires improving the powder dispersibility to ensure highly efficient drug delivery to the lung (5, 10). The dispersibility of microparticle-based powders is directly related to the interaction forces between particles. Four major inter-particle forces are the main barriers to overcome in designing dispersible aerosol particles for inhalation (11): mechanical interlocking due to surface asperities, capillary forces from the presence of water, electrostatics arising from the insulating nature of the material, and van der Waals forces resulting from the fundamental electromagnetic nature of matter. From a practical point of view, material properties of the formulated components such as solid phases, surface energy, dielectric properties, and particle attributes such as size distribution, morphology, shape, surface area, surface roughness, and moisture content, are some of the key variables that need to be carefully designed to improve the final powder dispersibility. Improved physical and chemical stability is another important aspect of inhalation formulation development (5, 12).

In addition, state-of-the-art inhaled formulation design is seeing an increasing emphasis on developing new particle engineering strategies and novel excipients to achieve the best pulmonary drug delivery

outcome (9, 12). Spray drying is a highly-customizable particle engineering technique that has been widely used to convert liquid feedstocks to solid powders by drying atomized feedstock droplets in a controlled drying environment (13). It has gained popularity in inhaled formulation manufacturing because it allows for accurate control of the various particle attributes in a one-step drying process. Novel excipients are likewise of great interest and in high demand in modern inhalation formulations for the delivery of various therapeutics (14). Excipients carefully selected according to various predefined criteria can not only improve the dispersibility and stability of the formulation but also add specific functionalities such as protection and stabilization of the active drugs, targeted delivery, and controlled release (14). Excipients may be used as external carrier particles that are usually blended with the fine cohesive drug particles in dry powder inhaler formulations to improve the handling, dispersing, and metering of the potent drugs. Alternatively, they can be directly formulated with the drug substances during manufacturing processes such as spray drying to form composite particles with desirable attributes (14-16).

Sugars, amino acids, and lipids are three of the most common excipient types used in inhalation formulations and many are 'generally recognized as safe' (GRAS) by the Food and Drug Administration Agency (FDA) (17). Lactose is the most commonly used sugar excipient in DPI formulations due to its physico-chemical stability, safety, compatibility with drug substances, inertness, and low cost and is typically used in the form of coarse carrier particles (18). However, amino acid-based excipients, such as leucine, trileucine, glycine, alanine, and histidine, are frequently used during manufacturing to form composite drug particles for improved stability and dispersibility (14, 19). Lipid-based excipients are one of the most extensively investigated systems for inhaled drug delivery to the lungs because of their easy processability, broad accessibility, and excellent biocompatibility (20, 21). Lipid excipients in inhalation formulations have been engineered into different formats, including nano or micro-emulsions, lipid nanoparticles, liposomes, and lipid microparticles. Most of these have been primarily dispersed in a liquid medium and delivered by nebulization when targeting the lung (22). Standing as an exception, lipid microparticles can be directly inhaled without relying on a second liquid medium and have been proven a promising constituent in pMDI and DPI formulations (23).

Of the various lipid-based microparticles proposed for inhaled drug delivery applications in the literature, most were prepared by spray drying (22, 24). Vanbever et al. spray dried respirable porous particles consisting of albumin, lactose, and DPPC (dipalmitoyl phosphatidylcholine) from an ethanolic solution and achieved high powder dispersibility when the formulation was tested in an Spinhaler^{TM} DPI (25). A series of follow-up studies by Vanbever et al. further compared the effect of different excipients, including DPPC, on powder aerosolization performance (26, 27). Suspended tobramycin and dissolved lipids, including cholesterol, DPPC, and DSPC (distearoyl phosphatidylcholine), in isopropanol were spray dried by Pilcer et al. to produce dispersible lipid-coated particles for dry powder inhalation (28). A multi-component polymer-lipid microparticle system combining morphology modifiers (polyvinyl alcohol), aerosolization enhancers (l-leucine), mucoadhesives (chitosan), and natural components (DPPC) was engineered by spray drying and tested *in vitro* by Eleftheriadis et al. (29). Shetty et al. coated an active drug excipient with different types of lipidic excipient, including DPPC, DPPG (dipalmitoyl phosphoglycerol), DSPC, and DSPG (distearoyl phosphoglycerol), by spray drying their solutions in an organic solvent, and reported different levels of improvement to aerosol performance (30). Because of the low solubility of lipids in water, most lipid microparticle production processes require organic solvent, which raises some concerns about safety and manufacturability.

Inhalable lipid microparticles manufactured without the use of organic solvent are available. For instance, solid lipid microparticles made from glyceryl behenate and loaded with the bronchodilator salbutamol (31, 32) and the corticosteroid budesonide (33) have been prepared using a melt emulsification method, with the final products demonstrating promising *in vitro* aerosol performance and potential for controlled release inhalation therapy. Similar manufacturing methods have also been applied to other lipids such as tristearin and stearic acid for the incorporation of different therapeutics, including quercetin and rifampicin (34, 35). Standing out from among these lipid-based excipient systems is the PulmoSphere™ platform, which consists of small, highly porous sponge-like DSPC particles prepared by emulsion-based spray drying (36). The key to producing PulmoSphere™ particles lies in the feedstock preparation step, in which a perflubron (PFOB)-in-water emulsion feedstock is prepared by multiple passes of high-pressure homogenization using DSPC as the emulsion stabilizer (36). The PFOB oil droplets act as a place-holder for pores in the particle and are completely evaporated during and after spray drying, leaving particles with extremely high porosity and low density. Active drug substances can be incorporated into the porous particles in solution-based, suspension-based, or carrier-based formats (37). This porous particle platform has been applied not only to DPI formulations (38, 39) but also, in modified form, to pMDIs (40, 41) with excellent adaptability and performance, resulting in the successfully commercialized DPI product Tobi® Podhaler® (Novartis) and pMDI products Bevespi and Breztri Aerosphere® (AstraZeneca).

Of the different types of lipid excipients used in the preparation of inhalable microparticles, it is obvious that phosphatidylcholines (PC), including the aforementioned DPPC and DSPC, are the most favorable because, in addition to the general advantages of lipidic excipients, they are endogenous to the lungs and represent a significant fraction of the total lipids in the lung (65%) and lung surfactant (90%) (42). This inherent endogeneity is valuable for efficient pulmonary drug transportation because inhaled drug particles deposited deep in the lungs are first confronted by a thin (10-20 nm) phospholipid-rich surfactant-lining fluid layer before going through either absorptive or non-absorptive clearances (43). In comparison to the other natural lipids, they also have fairly high lipid phase transition temperatures and relatively stable molecular structures that can be further stabilized through the addition of counterions such as Ca^{2+} (44). This fact is important because, in the manufacture of lipid microparticles for inhalation, the different lipid phases and the transitions between them are believed to be critical to the particle formation processes, which can in turn affect the processability and stability of the resulting product. Miller et al. pointed out that DSPC, with its relatively higher main phase transition temperature, was intentionally selected over other PC lipids for the production of the tobramycin-loaded PulmoSphere™ porous particles to enable better control of the particle formation during spray drying and also ensure high stability of the product (39). In a recent study by Corzo et al., lipid phase diagrams were used to help set the processing condition boundaries during spray drying (45). The direct relation between lipid phase transition temperature and spray drying outlet temperature was believed to strongly affect the particle formation process and eventually the processability of the product (45). Therefore, having a basic understanding of the lipid phases and potential transitions is an important preliminary step in developing new lipid microparticles intended for inhalation applications. The lipid phases in an aqueous environment are of particular interest, not only for their role in the rational development of new manufacturing processes but also for the increased understanding they offer of the fate of lipids from formulation preparation to storage and even to the final drug delivery.

Most PC lipids consist of amphiphilic molecules with a hydrophilic polar headgroup in addition to hydrophobic hydrocarbon chains. When hydrated, they display both thermotropic and lyotropic

mesomorphism and can lead to very complex phase diagrams with various lipid phases (46, 47). Only four of the most encountered lipid phases as listed in **Table I** are discussed here. Hydrated medium-chain length phosphatidylcholines such as DPPC and DSPC can undergo a series of transitions between different phases with increasing temperature. Briefly, long-time incubation at low temperatures leads to a stable crystalline phase (L_c) that can then convert to a gel phase with tilted chains ($L_{\beta'}$) at an elevated subtransition temperature T_s. The $L_{\beta'}$ gel phase can further convert to a rippled gel phase ($P_{\beta'}$) at the pretransition temperature T_p, while most phospholipids can skip the pretransition and convert directly to the short-range disordered liquid crystalline phase L_α at the main transition temperature T_m (46-48). The subtransition and pretransition steps for hydrated lipids can sometimes be difficult to identify, while the main phase transition temperature, sometimes also called the chain-melting transition temperature, marks the distinct transition point of the hydrated lipid from ordered to disordered chain structure. Lipid molecules above the main transition temperature are believed to have a remarkably increased level of mobility (49). This is why hydrated phospholipid vesicles are usually considered 'solid' at temperatures below T_m but are treated as 'fluid' at temperatures above T_m (50). For these reasons, the lipid main phase transition temperature was hypothesized as the key parameter in the design of new manufacturing processes for lipid microparticles, as well as in the structure of the final particle.

$$L_c \xrightarrow{T_s} L_{\beta'} \xrightarrow{T_p} P_{\beta'} \xrightarrow{T_m} L_\alpha$$

Table I Nomenclature for the most common lipid phases

Nomenclature	Long-range order	Short-range chain order	Phase
$\mathbf{L_c}$	one-dimensional lamellar	ordered	subgel/crystalline phase
$\mathbf{L_{\beta'}}$	one-dimensional lamellar	partially ordered	gel phase with tilted chains
$\mathbf{P_{\beta'}}$	two-dimensional oblique or centered	partially ordered	rippled gel phase
$\mathbf{L_\alpha}$	one-dimensional lamellar	disordered	liquid crystalline phase

The considerable promise of respirable solid lipid microparticles designed with PC lipids for pulmonary drug delivery applications provided strong motivation for this study. In it, we present a new spray drying method with a simplified feedstock preparation process to produce rugose PC lipid particles that can be used as a platform for applications designed for, but not limited to, respiratory drug delivery.

MATERIALS AND METHODS

Materials

Feedstock preparation and spray drying processes for the saturated phosphatidylcholine 1,2-distearoyl-*sn*-glycero-3-phosphocholine (DSPC or 18:0 PC; 850365, Avanti Polar Lipids Inc., AL, USA) were first investigated in this study. Calcium chloride dihydrate ($CaCl_2$•$2H_2O$, Sigma-Aldrich, ON, Canada) was added during feedstock preparation to stabilize the liquid dispersion against flocculation (36, 38).

Two other PC lipids were also investigated as alternatives to DSPC: 1,2-diarachidoyl-sn-glycero-3-phosphocholine (DAPC or 20:0 PC; 850368, Avanti Polar Lipids Inc., AL, USA) and 1,2-dibehenoyl-sn-glycero-3-phosphocholine (22:0 PC; 850371, Avanti Polar Lipids Inc., AL, USA). The molecular structures of all three phospholipids are very similar, with two long hydrophobic saturated fatty acid tails attached to a hydrophilic phosphatidylcholine head-group. However, the chain length of the attached fatty acid tails varies from 18 to 22, resulting in different properties, including increased main phase transition temperatures as listed in **Table II**.

Table II Molecular structures, chain lengths and main phase transition temperatures for the phosphatidylcholines investigated in this study.

Lipid	18:0 PC (DSPC)	20:0 PC (DAPC)	22:0 PC
Full name	1,2-distearoyl-sn-glycero-3-phosphocholine	1,2-diarachidoyl-sn-glycero-3-phosphocholine	1,2-dibehenoyl-sn-glycero-3-phosphocholine
Molecular formula	$C_{44}H_{88}NO_8P$	$C_{48}H_{96}NO_8P$	$C_{52}H_{104}NO_8P$
Molar mass (g/mol)	790.2	846.3	902.4
Main phase transition T_m (°C)	55	66	75

Methods

Spray drying of DSPC particles

The feedstock preparation method for the spray drying of DSPC lipid particles is illustrated in **Fig. 1**. Pure water was first heated to 55 °C, that is, close to the main phase transition temperature of DSPC, using a hotplate equipped with a feedback temperature control. Calcium chloride dihydrate and DSPC lipid were then added to the heated water at a molar ratio of 1:2 to a targeted total solids concentration of 20 mg/mL. After gentle shaking of the dispersion to fully immerse the added solids, the obtained translucent feedstock was kept on the hotplate for another 30 minutes, before undergoing a high shear mixing process in which the dispersing probe (S18N-19G, IKA, NC, USA) of a high shear mixer (T-18 Ultra-Turrax, IKA, NC, USA) was immersed into the liquid sample to mix and disperse the feedstock for 3 minutes at 25,000 rpm. A slight fluctuation in the feedstock temperature (±3 °C) was observed during the preparation process due to the heat introduced by high-shear mixing. A small aliquot of the feedstock was extracted after the mixing process, dropped on a Petri dish, dried under vacuum, and transferred for electron microscopy analysis. The feedstock was then supplied to a twin-fluid atomizer for spray drying using a peristaltic pump (Masterflex® L/S®, Cole-Parmer, QC, Canada) while continuing to be heated and with the high-shear dispersing probe still immersed in the liquid and operating at ~5000 rpm to prevent flocculation. Since the tubing was not thermostated, the feedstock experienced a temperature drop as it was fed through and was then reheated in the atomizer just prior to atomization.

A custom-built modular lab-scale spray dryer (51) was used to spray dry all formulations in this study. A fixed feed flow rate of 2.5 mL/min and a drying gas flow rate of 600 SLPM were used for all spray drying runs. The atomizer gas flow rate was set to ~20 L/min so that the twin-fluid atomizer operated at an air-liquid ratio of 10, corresponding to a mass median initial droplet diameter of approximately 9.0 µm (52). Particle size distributions of the dried particles were measured in-process using a combination of an

isokinetic sampling probe (51), an aerosol diluter (3302A, TSI, MN, USA), and a time-of-flight aerodynamic particle sizer (APS, 3321, TSI, MN, USA) placed close to the outlet of the spray dryer as indicated in **Fig. 1**.

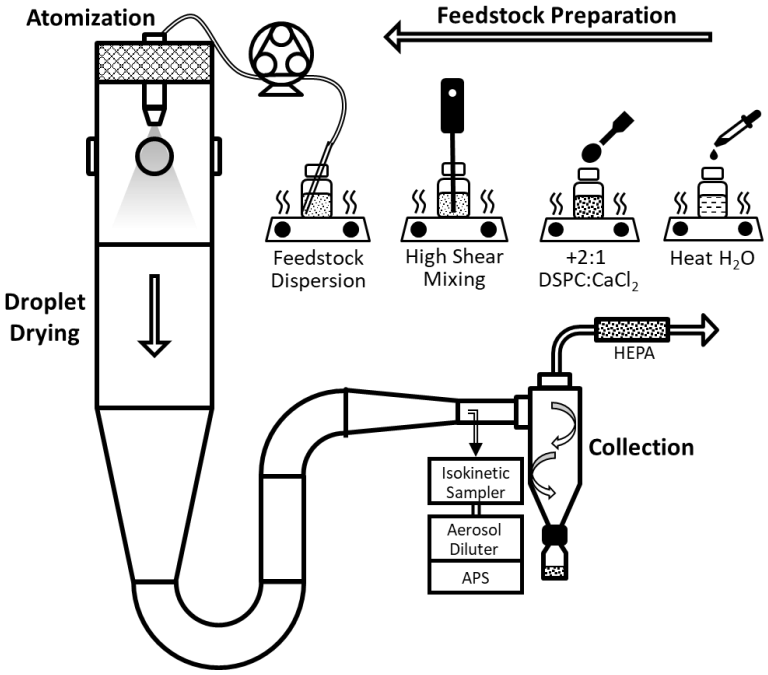

Fig. 1 Schematic illustration of the feedstock preparation and spray drying processes used in this study.

Heat loss experiments combined with spray dryer process modeling (53) were used to predict the temperature and relative humidity at the outlet of the dryer under different processing conditions. An inlet temperature of 75 °C, which corresponded to a predicted outlet temperature of 50.1 °C, was selected for the spray drying of the DSPC lipid particles in order to keep the dryer outlet temperature below the main phase transition temperature of DSPC at 55 °C as listed in **Table II**. Relative humidities at the outlet of the dryer were also predicted, with the results listed in **Table III**. Particles collected by a stainless-steel cyclone were further dried under vacuum at room temperature for more than 24 hours to remove residual moisture content. Particles from this batch were treated as the control case (#6 in **Table III**) and compared with particles from varying batches.

Variation of factors affecting particle morphology

Processing conditions were optimized to achieve the highest particle rugosity. The feedstock temperature (T_{feed}), the spray drying outlet temperature (T_{out}), and their relation to the lipid phase transition temperature were hypothesized to be important in determining the dried particle morphology and structure. To study the effect of these factors on the final particle morphology, an experimental matrix that spanned both feedstock and outlet temperatures across the main phase transition temperature of DSPC was designed and is shown as cases #1-9 in **Table III**.

More specifically, to study the effect of feedstock temperature on particle rugosity, in addition to the control case two more spray drying runs with the same inlet temperature of 75 °C but different feedstock temperatures were designed. These are listed in **Table III** as batch #1, with a lower T_{feed} (40 °C), and batch #9, with a higher T_{feed} (65 °C) than the main phase transition temperature of DSPC. To study the effect of the spray drying outlet temperature on particle rugosity, six more spray drying runs with the same T_{feed}

(55 °C) but different spray drying inlet temperatures (35, 45, 55, 65, 90, 120 °C) were added as cases #2, 3, 4, 5, 7, and 8 in **Table III**, with the corresponding predicted outlet temperatures ranging from below the T_m of DSPC at 24.9 °C to above the T_m up to 78.4 °C. Specific surface areas (*SSA*) of the dried particles were measured and used to calculate particle rugosity. Spray drying yield was used to assess the processability of the different batches.

To eliminate the potential effect of cyclone collection on particle morphology at high spray drying outlet temperatures, a custom-designed single-nozzle impactor (54) operated at 5 L/min and a two-stage configuration—top stage with a 6.7 µm cutoff aerodynamic diameter that acted as a pre-separator and bottom stage with a cutoff diameter of 1.3 µm—was used as an in-line particle sampler to extract particles from batch #8 (RLP-55T_f-120T_{in}) for SEM imaging. The sampling probe was connected to the dryer right before the cyclone at a location similar to the one used for the particle size measurement, as shown in **Fig. 1**.

Table III Phospholipid particle spray drying experimental matrix with the corresponding spray drying processing conditions and predicted outlet temperature ($T_{out,p}$). A fixed solids concentration of 20 mg/mL, feed flow rate of 2.5 mL/min, and drying gas flow rate of 600 SLPM were used for all the cases. Batch #6 (bolded) was used as the control case.

Batch #	Lot	Lipid	T_{feed}(°C)	T_{in}(°C)	$T_{out,p}$(°C)	$RH_{out,p}$(%)
1	RLP-40T_f-75T_{in}	DSPC	40	75	50.1	6.2
2	RLP-55T_f-35T_{in}		55	35	24.9	23.2
3	RLP-55T_f-45T_{in}			45	31.2	16.3
4	RLP-55T_f-55T_{in}			55	37.5	11.6
5	RLP-55T_f-65T_{in}			65	43.8	8.5
6*	**RLP-55T_f-75T_{in}**			**75**	**50.1**	**6.2**
7	RLP-55T_f-90T_{in}			90	59.6	4.1
8	RLP-55T_f-120T_{in}			120	78.4	1.9
9	RLP-65T_f-75T_{in}		65	75	50.1	6.2
10	RLP-65T_f-95T_{in}	DAPC	65	95	62.7	3.5
11	RLP-75T_f-110T_{in}	22:0 PC	75	110	72.1	2.4

Dynamic light scattering

To better understand the feedstock properties, the mean hydrodynamic diameter and polydispersity index of the DSPC lipid particles dispersed in the liquid feedstock were measured after high shear mixing using a dynamic light scattering instrument (ZetaSizer Nano, Malvern, UK). During the pumping process for the feedstocks prepared at different temperatures (T_{feed} = 40, 55, 65 °C) from batches #1, #6, and #9, roughly 1 mL of liquid sample was extracted from the bulk feedstock for each case and transferred for immediate measurement. All samples were measured at a temperature of 25 °C from a fixed position of 3 mm from the bottom of the cuvette, at a backscattering angle of 173°. Each measurement took approximately 1-3 minutes. Since volume or intensity-based size distributions were more sensitive to randomly detected large lipid aggregates, number size distributions that showed better consistency between repeated measurements and across samples were used for clearer comparison. The reported average and standard deviation of the size distribution statistics for each formulation are from the same sample, analyzed three times. The polydispersity index as a measure of the width of the size distribution

was calculated as the square of the standard deviation of the measured size distribution divided by the mean diameter.

Particle morphology analysis

Micrographs of the collected particles were obtained either by a scanning electron microscope (Evo M10, Zeiss, Germany) for general morphological analysis, or by a field emission scanning electron microscope (Sigma FESEM, Zeiss, Germany) for high-resolution studies. To eliminate charging effects, particles were first loaded onto standard SEM pin mounts (16111, Ted Pella Inc., CA, USA) with double-sided adhesive carbon tape as a substrate and coated for 2 minutes with gold nanoparticles to a thickness of approximately 16 nm using a sputter coater (Desk II, Denton Vacuum, NJ, USA). A low accelerating voltage of 5 kV was used for all cases to prevent potential electron beam damage to the lipid particles.

Specific surface area and rugosity

To quantitatively compare the different morphologies of the spray-dried powders, their specific surface areas were determined by measuring the adsorption isotherm of nitrogen gas to the particles with a gas sorption analyzer (Autosorb 1MP, Quantachrome Instruments, FL, USA) and then analyzing the results with a 7-point BET (Brunauer-Emmett-Teller) method (55). For each test, 0.1 - 0.2 g of the spray-dried powder was first loaded into a sample cell (O.D. = 6 mm) and degassed at room temperature for >6 hours. Nitrogen was used as the adsorbate gaseous phase and was assumed to have a single-molecule cross-sectional area of 16.2 $Å^2$. The nitrogen physisorption analysis was then conducted for a relative pressure (P/P_0) range of 0.05 - 0.35 at the boiling temperature of liquid nitrogen at -196 °C. Good linearities (correction coefficient $R^2 > 0.99$) were observed for all the samples during the analysis of their 7-point nitrogen adsorption isotherms.

Solid spherical particles with true density of the material (ρ_t) are assumed for the definition of geometric specific surface area (A_g). Since all spray drying runs used a fixed feedstock concentration (c_0) of 20 mg/mL and the same atomizer settings for the same initial droplet size (d_0), volume equivalent diameters (d_V) for such hypothetical solid particles can be calculated by the following equation:

$$d_V = \sqrt[3]{\frac{c_0}{\rho_t}} \cdot d_0 \quad (1)$$

The powders were therefore expected to have the same geometric specific surface area, which was defined according to the particle volume-equivalent diameter and calculated using **Eq. 2**:

$$A_g = \frac{\pi d_V^2}{\frac{1}{6}\rho_t \pi d_V^3} = \frac{6}{\rho_t d_V} \quad (2)$$

The rugosity of the particles (f_r) was calculated as the ratio of the measured real specific surface area (A_r) to the theoretical geometric surface area (A_g) using **Eq. 3**:

$$f_r = \frac{A_r}{A_g} = \frac{1}{6}\rho_t d_V A_r \quad (3)$$

Aerosol performance characterization

Aerosol performance for two of the spray dried powders from **Table III**, control batch #6 and batch #4 (the latter spray dried at a lower temperature), was tested. A commercial low-resistance dry powder

inhaler device (Seebri Breezhaler, Novartis) in combination with a Next Generation Impactor (NGI, Copley Sci. Ltd., UK) was used to evaluate the aerosolization performance of the spray dried powders *in vitro*. A similar setup has been described in detail elsewhere (56). Briefly, an Alberta Idealized Throat (AIT) was mounted to the inlet of the impactor to assess particle deposition in the human extrathoracic region under normal use. All NGI plates and the interior of the AIT were cleaned and coated with silicone spray (Molykote 316, Dow Corning Corp., MI, USA) and dried for more than 30 minutes before each use to reduce particle bouncing. A critical flow controller (TPK 2000, Copley Sci. Ltd., UK) connected to a vacuum pump was used to simulate a square inhalation flow profile. The testing flow rate was set to 100 L/min, as recommended by the USP-601 monograph for low-resistance DPI devices with a pressure drop less than 4 kPa (57). Each inhalation was simulated for 2.4 s, corresponding to a 4 L inhalation volume. Powders were first filled into size-three hydroxypropyl methylcellulose capsules (Quali-V-I, Qualicaps Inc., IN, USA) in a dry environment (< 0.1% relative humidity), which were then pierced by the DPI device upon actuation. Each capsule contained 23.3 ± 4.5 mg powder, and three capsules were actuated per test to obtain sufficient mass on the impactor stages for subsequent gravimetric analysis. Experiments were performed under ambient conditions in triplicate for each set of samples.

Two main parameters, the emitted dose (ED) and total lung dose (TLD), were assessed from the *in vitro* measurements for the selected lipid particles. The emitted dose, defined as the percentage of powder emitted from the loaded DPI, was calculated based on the mass of loaded powder in each capsule and the DPI mass before and after actuation. The total lung dose was determined as the percentage of powder loaded in the capsule that bypassed both the actuator and AIT to be collected on the impactor stages. The *in vitro* data collected from the NGI was used as the input for a regional lung deposition model to estimate the particle deposition in each generation of a symmetric lung model, which consists of 23 generations (58). A detailed description of the regional lung deposition model is available elsewhere (59, 60). Briefly, particle deposition via three mechanisms—inertial impaction, sedimentation, and diffusion—was modeled for three phases of a full breathing cycle, including inhalation, breath-hold, and exhalation. An inhalation time of 1.6 seconds, a constant inhalation flow rate of 100 L/min, a breath-hold of 10 seconds and an exhalation time of 7 seconds were used for the simulation. Calculated regional lung deposition results in terms of tracheobronchial deposition—which was defined as the summed particle depositions in generations 0 to 14 of the lung model—and alveolar deposition—which represented particles deposited in generations 15 to 23—in percent of the emitted dose and *in vitro* lung dose were presented. Exhaled dose of the modeling results was counted towards the alveolar deposition as the exhaled doses for single breath inhalers are usually negligible and this approach best aligned with our experimental method, in which there can be no exhaled fraction of the emitted aerosol (60).

Spray drying of long-chain lipids

The newly developed method was also applied to the spray drying of two different lipids, DAPC and 22:0 PC, both of which have the same molecular structure as DSPC but longer chain lengths and higher main phase transition temperatures (**Table II**). The same processes, including the heating of pure water on a hotplate, the addition of lipid and $CaCl_2$ at a molar ratio of 2:1, and the use of high shear mixing, were implemented. As listed in **Table II**, the applied feedstock preparation temperature was adjusted to 65 °C and 75 °C to match the respective main phase transition temperature of each lipid. The spray drying inlet temperature for DAPC and 22:0 PC was also increased to 95 °C and 100 °C, respectively, so that the predicted dryer outlet temperatures (62.7, 72.1 °C) dropped slightly below the respective lipid main phase transition temperatures.

RESULTS AND DISCUSSION

Particle morphology

The feedstock for control batch #6 was kept heated throughout the entire preparation process. It was noted that the volume of the feedstock increased rapidly at the beginning of the high shear mixing process as air became trapped in the liquid and led to foaming. Subsequently, the volume of the liquid feedstock decreased to close to its initial state, probably because the high shear mixing disrupted the air bubbles. An opaque, milk-like liquid feedstock was obtained at the end of the process. The morphological transition of the DSPC lipid from its original raw material state to the final dried particle state was monitored by SEM, with the resulting micrographs presented in **Fig. 2**. It can be observed that prior to feedstock preparation most raw lipid materials were in the form of large broken sheets with very smooth surfaces and sharp edges, as shown in **Fig. 2**(a). Some of the larger lipid sheets had dimensions longer than 20 µm and thicker than 2 µm.

In contrast, **Fig. 2**(b) presents a feedstock dispersion that had undergone 3 minutes of high shear mixing at 55 °C and was subsequently dried on a Petri dish. This dried dispersion shows significant differences from the original raw lipid morphology in **Fig. 2**(a). Highly wrinkled surfaces on composite structures with many open pores can be observed. Representative results from dynamic light scattering measurements of the feedstock after high-shear mixing, presented in **Fig. 3**(b), show a predominance of lipid nanoparticles in the 100nm size range. Since the feedstock was prepared at a temperature close to the main phase transition temperature of the lipid, it was concluded that a considerable fraction of the raw lipid material with the coarse morphology shown in **Fig. 2**(a) went through the main phase transition and formed the more mobile liquid crystalline phase, which was then disrupted into smaller lipid fragments by the high shear rate of the mixing process.

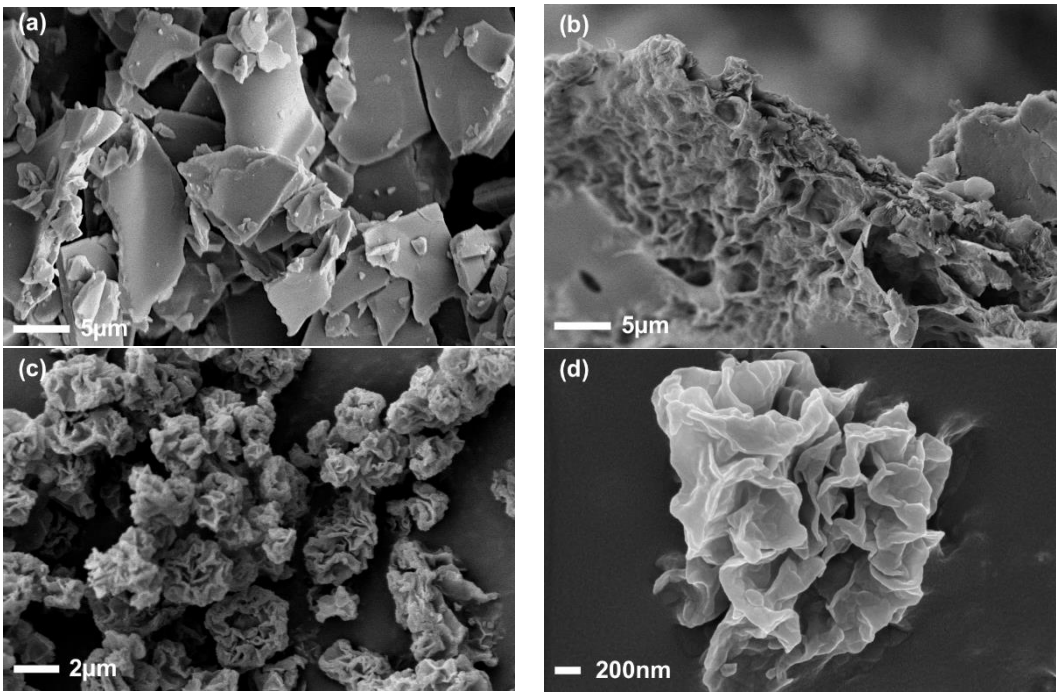

Fig. 2 Morphology of (a) raw DSPC lipid material; (b) feedstock dispersion dried on a Petri dish; (c)-(d) highly rugose DSPC lipid particles (batch #6, RLP-55T_f-75T_{in}) after spray drying.

Lipids dispersed in water can rearrange themselves into different formats such as micelles, lipid bilayer sheets, liposomes, and so on, covering a wide size range from spherical micelles in the 10 nm range (61) to small unilamellar vesicles (SUV < 100 nm), large unilamellar vesicles (LUV > 100 nm), and even larger multilamellar vesicles (LMV) or lipid bilayer sheets (50). The solubility of phosphatidylcholines in water is highly dependent on the hydrocarbon chain length, with long-chain lipids like DSPC, DAPC, and 22:0 PC all being considered effectively insoluble in water (47, 62). Therefore, it was assumed that no free lipid molecules were present in the feedstock. The exact forms of the dispersed lipids present in the feedstock could not simply be concluded from the size distribution; rather, a mixture of multiple formats was likely, given the presence of larger lipid particles higher in the micrometer range that were primarily apparent in the volume-based size distributions (data not shown). Given that the feedstock preparation temperature was intentionally set close to the main phase transition temperature of DSPC for this case, some lipid may have remained in the gel phase and was only micronized to the micrometer range by the high shear mixer.

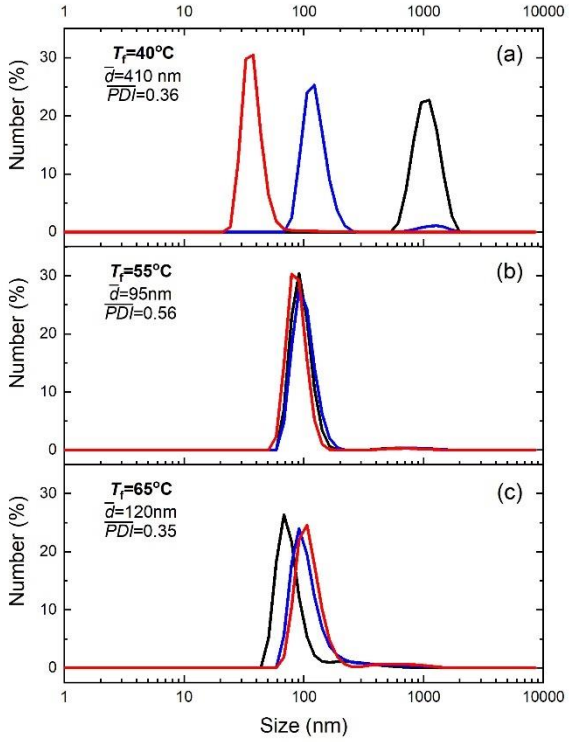

Fig. 3 Representative number size distributions of dispersed DSPC lipids in feedstocks prepared at different temperatures after high shear mixing: (a) T_{feed} = 40 °C, (b) T_{feed} = 55 °C, and (c) T_{feed} = 65 °C. The different lines for each sample stand for three consecutive measurements (dark to blue to red), with each measurement taking 1 - 3 minutes. $\overline{PDI}$ stands for average polydispersity index and $\overline{d}$ stands for average diameter of the three measurements.

The morphologies of particles spray dried from the control batch (#6 in **Table III**) with an inlet temperature of 75 °C and a feedstock temperature of 55 °C are presented in **Fig. 2**(c-d). No large pieces of lipid sheets were observed, indicating that the high shear mixing process was able to disrupt the DSPC lipids from their original state and led to the structural reformation. During the spray drying process, the measured dryer outlet temperature of 51.5 ± 0.5 °C (**Table IV**) was well predicted by the processing model (50.1 °C) to be just below the main phase transition temperature of DSPC, as designed. The lower-magnification micrograph **Fig. 2** (c) shows that the collected particles are within the optimal respirable range of 1-5 µm. This is well supported by the in-line particle size distribution measurement results in **Fig. 4**, which show that the particles from this batch had an *MMAD* of 2.1 µm and a *GSD* of 1.6. With the initial volume equivalent diameter ($d_{0,50}$) of the atomized droplets established as ~9.0 µm at the implemented air-liquid ratio of 10 (52), the particle density could be roughly estimated using **Eq. 4**, where measured particle aerodynamic diameter $d_{a,50}$=2.1 µm, feedstock solids concentration c_0=20 mg/mL, $d_{0,50}$ = 9.0 µm, and unit density ρ_0 = 1 g/cm^3. Assuming DSPC has a true density close to 1.1 g/cm^3, these particles had an estimated particle density of 0.4 g/cm^3, which corresponds to a porosity of ~65% for the particles observed in **Fig. 2** (c).

$$\rho_{\mathrm{p}} = \left(\frac{d_{a,50}}{d_{0,50}}\right)^6 \bullet \frac{\rho_0^3}{c_0^2} \tag{4}$$

Table IV Measured outlet temperatures ($T_{\mathrm{out,m}}$), yield, and specific surface areas (*SSA*) for all the spray drying batches. Particle rugosities (f_r) were all calculated using a solid particle density of 1.1 g/cm^3 and the same volume equivalent diameter calculated using **Eq. 1**. All batches had the same batch size of 0.5 g and a run time ≤ 10 min. Batch #6 (bolded) was used as the control case.

Batch #	Lot	Lipid	$T_{\mathrm{out,m}}$(°C)	Yield (%)	*SSA* (m^2/g)	f_r
1	RLP-40T_f-75T_{in}	DSPC	52.5±0.5	10	-	-
2	RLP-55T_f-35T_{in}		25.4±0.2	50	10.7	4.6
3	RLP-55T_f-45T_{in}		32.5±0.2	70	9.5	4.1
4	RLP-55T_f-55T_{in}		38.5±0.5	80	8.6	3.7
5	RLP-55T_f-65T_{in}		44.0±0.5	74	15.7	6.8
6*	**RLP-55T_f-75T_{in}**		**51.5±0.5**	**72**	**18.3**	**7.9**
7	RLP-55T_f-90T_{in}		58.7±0.5	70	6.2	2.7
8	RLP-55T_f-120T_{in}		74.2±0.5	68	3.1	1.4
9	RLP-65T_f-75T_{in}		50.1±0.5	78	5.9	2.6
10	RLP-65T_f-95T_{in}	DAPC	62.0±0.5	72	9.1	4.0
11	RLP-75T_f-110T_{in}	22:0 PC	71.4±0.5	74	6.9	3.0

Furthermore, the dried lipid particles showed a composite structure with high rugosity, which has been demonstrated to be a key feature of highly dispersible particles with good aerosol performance (63, 64). A large specific surface area of 18.3 m^2/g was recorded for these particles. Using the estimated 1.1 g/cm^3 as the lipid true density for the volume equivalent diameter calculation according to **Eq. 1**, this batch of particles had an estimated rugosity of 7.9 according to **Eq. 3**, meaning that the produced rugose lipid particles (RLP) had almost eight times the surface area than particles with the same volume equivalent diameter but with smooth surfaces. Considering the small batch size (0.5 g) and short run time (< 10 min)

used for this spray drying run, the 72% yield achieved for this batch was very promising and indicated good manufacturing potential for the new lipid microparticle system.

Since the lipid in the feedstock was mostly in the form of a nanoparticle suspension, the formation process for these rugose lipid particles was expected to be diffusion controlled. According to the applicable particle formation models in spray drying (65), the Péclet number—defined as the ratio of the evaporation rate, κ, of the continuous phase to the diffusion rate of the dispersed solid, D, i.e., $Pe = \kappa/8D$—was very high for the nanoparticles detected in the 100 nm range. These lipid nanoparticles were predicted to accumulate quickly on the droplet surface, aggregate there, and form a shell. This shell may then deform or collapse later in the evaporation process through the influence of surface tension, a process that affects rugosity and likely depends on temperature, which determines the mechanical properties of the lipid. The higher magnification micrograph, **Fig. 2**(d), shows that the particles were made of fused thin lipid sheets instead of loosely aggregated fragments, probably because a fraction of the lipid was present in the more mobile liquid crystalline phase. Particles with such highly folded, rough surfaces are favorable for drug loading, either through adhesion of drug crystals or through the incorporation of micronized drugs into the feedstock (37, 41).

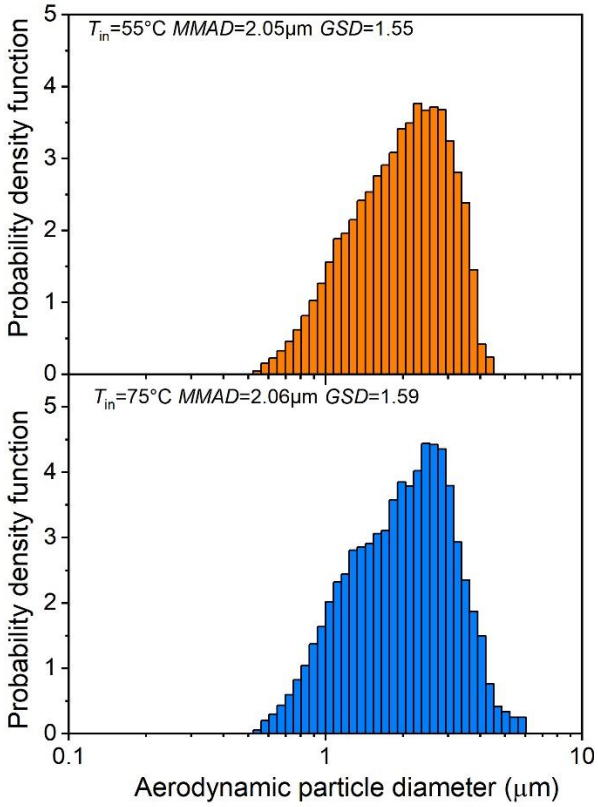

Fig. 4 Isokinetically measured primary particle size distributions of spray-dried lipid particles for two selected batches, #4 (RLP-55T_f-55T_{in}) and #6 (RLP-55T_f-75T_{in}). The two batches show similar size distributions with the same *MMAD* of 2.1 μm and a *GSD* of 1.6.

Effect of feedstock temperature on particle morphology

From the internal structures of the solids dried from the liquid feedstock dispersion presented in **Fig. 2** (b) and the rugose lipid particles collected from spray drying shown in **Fig. 2** (c-d), it was further hypothesized that the feedstock temperature in relation to the main phase transition temperature of the lipid is an important processing parameter for the production of the desired rugose particle morphology. To study the effect of feed temperature on the final particle morphology, spray drying batches #1, 6, and 9 in **Table III** were manufactured using a fixed spray drying inlet temperature of 75 °C but a wide range of feedstock temperatures: 40 °C, 55 °C, and 65 °C, respectively. The yield for batch #1 (10%), produced at the lowest feedstock temperature, was much lower than the yields for the other two cases (72% for #6 and 78% for #9) because the feedstock in this case creamed during high shear mixing and converted into a foamed dispersion with high viscosity that couldn't be effectively pumped to the atomizer, as the picture of the foamed feedstock shows in **Fig. 5**. Only a small amount of powder was collected for SEM imaging, and the specific surface area was deemed not worth assessing because of the sample's poor manufacturability.

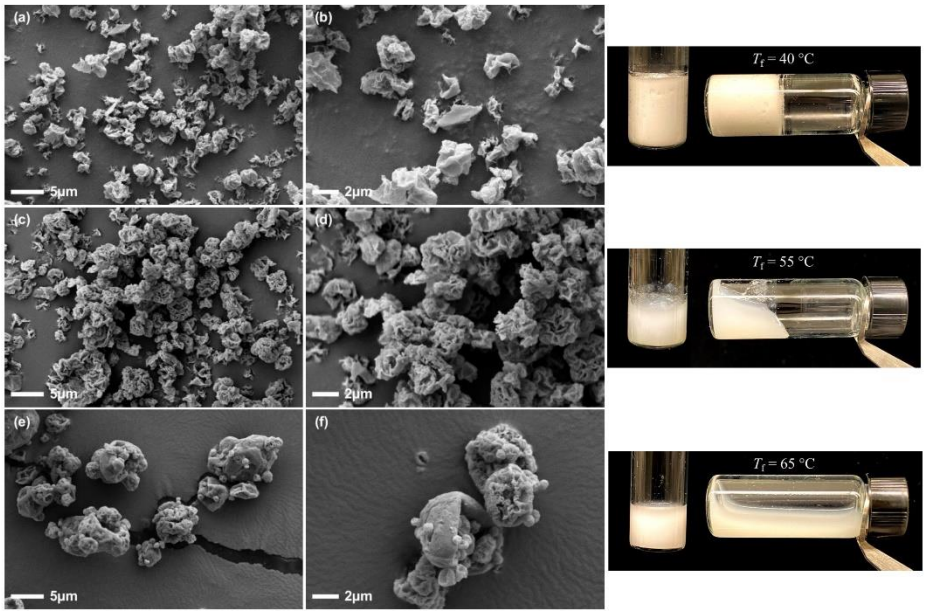

Fig. 5 Micrographs of particles from spray dried batch #1 (a-b, RLP-40T_f-75T_{in}), #6 (c-d, RLP-55T_f-75T_{in}), and #9 (e-f, RLP-65T_f-75T_{in}) show the dependence of particle morphology on feedstock preparation temperature. Pictures on the right show the different states of the corresponding feedstock emulsions when cooled down to room temperature.

In general, particles from all three cases still show corrugated surface morphologies regardless of feedstock temperature. However, in comparison to the highly rugose particles from the control batch shown in **Fig. 5** (c-d), the particles produced from a lower feedstock temperature at 40 °C shown in **Fig. 5** (a-b) appear less folded. Some of them consist of thin sheets with smooth surfaces. Particles presented in **Fig. 5** (e-f) are from batch #9, prepared at a T_{feed} of 65 °C. Highly rugose features can still be detected, albeit not consistently; instead, some particles have rather smooth surfaces with only minor folding. The morphological differences between these three batches indicate that the particles have the highest rugosity when the feedstock temperature is close to the lipid main phase transition temperature. Shifting away from this optimum temperature range led to less rugose particles and issues with manufacturability.

This observation is supported by the much lower *SSA* (5.9 m^2/g) and rugosity (2.6) for batch #9 than for control batch #6 as listed in **Table IV**.

The representative dynamic light scattering results presented in **Fig. 3**(a) prove that the lipid feedstock prepared at 40 °C was indeed very unstable. The main peaks of the presented number size distributions drifted quickly downwards from ~1 μm to < 50 nm from the first to the last measurement, indicating rapid flocculation of the large lipid particles. This drop occurred because the light scattering measurement position was at a fixed height (3 mm) from the bottom of the sample cuvette, so that flocculated and aggregated lipid particles quickly migrating upwards in the liquid feedstock out of the light scattering zone could no longer be measured. When prepared at temperatures far below the DSPC main phase transition temperature, the lipids were not able to go through the chain-melting transition to form the mobile liquid crystalline phase but instead remained in the gel phase. The high shear mixing process was not able to effectively break all the lipids in the gel phase down to the 100 nm range, leaving relatively large lipid sheets dispersed in the feedstock; hence the unstable feedstock and particle morphology with much less surface folding. The feedstocks prepared at the higher temperatures of 55 °C and 65 °C showed much-improved stability as indicated by the consistent dynamic light scattering results. The relatively smooth particle surfaces produced from the feedstock prepared at 65 °C were the result of the feedstock temperature's being much higher than the main phase transition temperature of DSPC. Most of the dispersed lipids were able to go through the main transition to form the mobile liquid crystalline phase. The considerably increased mobility led to a greater rearrangement of lipid molecules during particle formation and thus to an eventual reduction in rugose surface features to minimize surface energy. The different states of the emulsions prepared at these temperatures after cooling down to room temperature shown in **Fig. 5** further proved the different mobility of the lipid molecules during feedstock preparation.

Effect of spray drying outlet temperature on particle morphology

From the above study on the effects of feedstock temperature on particle morphology, it would appear that the mobility of lipid molecules in the feedstock is important for the formation of highly rugose structures. However, shell deformation and folding occur late in the particle formation process; therefore, mobility of lipid molecules during these processes may also be very influential. Since the mobility of lipid molecules during particle formation is directly related to temperature, and since the lipid particles were exposed to the dryer outlet temperature for the longest time of any of the stages of the spray drying process, it was hypothesized that the outlet temperature should also be well-controlled for the successful production of highly rugose lipid particles. The outlet temperature was expected to be more important than the inlet temperature because, during the early stages of droplet evaporation, the temperature is always well below the main phase transition temperature due to evaporative cooling (39). To study the effect on particle morphology, batches #2-8 in **Table III** were designed to have the same processing conditions as the others except for the inlet temperatures and the corresponding outlet temperatures. As listed in **Table IV**, the actual measured outlet temperatures were all well-predicted by the processing model. A wide range of outlet temperatures, from below the main phase transition temperature of DSPC close to room temperature at 25.4 °C to above T_m at 74.2 °C, was tested.

As shown in **Fig. 6** (a-e), the particles from batches #2-5 (a-d) with spray drying outlet temperatures below the lipid main phase transition temperature were all similar to those in the control batch, #6 I, with all exhibiting highly rugose particle surfaces. No clear morphological differences could be identified between

the particles in these cases. Interestingly, once the dryer outlet temperature surpassed the lipid main phase transition temperature to 58.7 °C, the particles exhibited notably different morphology, as shown in **Fig. 6** (f) for batch #7. Some rugose particles were still detected, but many of the particles had relatively smooth surfaces. For batch #8, which had the highest T_{out} at 74.2 °C, even the occasionally rugose particles visible in batch #7 were no longer detected. Instead, as shown in **Fig. 6** (g), only solid lipid particles with relatively smooth surfaces were observed.

Specific surface area and rugosity values listed in **Table IV** further prove that all the batches with a T_{out} lower than the T_m (#2-6) consist of highly rugose lipid particles. For batches #2-4, particle rugosities were around–4 - 5 when the T_{out} was relatively low and far from the T_m. As the T_{out} was increased to within 10 °C of the T_m, the particles showed a further increase in rugosity to–7 - 8 for batches #5 and #6. However, once the T_{out} crossed the T_m, the particles immediately transitioned to relatively smooth surfaces, causing the lowest resultant particle rugosities for batches #7 and #8. The rugosity value for batch #7 is only slightly lower than the values for batches #2-4 mainly because, as shown in **Fig. 6** (f), this batch consisted of both rugose particles and particles with relatively smooth surfaces. The rugosity for batch #8, with the highest T_{out} at 74.2 °C, was close to unity, indicating that most of the particles were indeed close to solid with no internal voids.

The transition of particle morphology from highly rugose to relatively smooth at higher T_{out} verifies the hypothesis that it is the temperature-dependent molecular mobility that affects the final particle structure. However, the final particle morphology does not answer the question of whether the particles suffered structural collapse during particle formation or upon heat exposure in the cyclone and collector. To eliminate the potential effect of cyclone collection on particle morphology, particles from batch #8 (RLP-55T_f-120T_{in}) were sampled for SEM imaging in-process using the single-stage impactor. As shown in **Fig. 6** (h), the sample collected in-line exhibited solid lipid particles with smooth surfaces very similar to those collected from the cyclone as shown in **Fig. 6** (g). This similarity proves that the rugose particle surfaces were not modified by collisions with the cyclone wall, friction, or heat exposure in the cyclone and collection bottle caused by the rotating flow, but rather that they were already formed, having collapsed in the later stages of droplet drying. Thus, changing the collection method, e.g., by using a filter, would have no effect on particle morphology in this case. Despite being highly rugose, these particles were successfully collected by the stainless steel cyclone at high efficiency with no evidence of milled or crushed particles observed, further proving a good manufacturability of this lipid platform.

The temperature-dependent nature of particle morphology in the spray drying of lipid-based microparticles is consistent with the findings reported in the literature (25, 45). It also explains the solid lipid particles with smooth surfaces produced at high spray drying outlet temperatures (26, 27) and the wrinkled lipid particles with irregular morphologies produced at low drying temperatures (66), especially in solution-based spray drying of lipid microparticles, where particles are formed completely from dissolved lipid molecules precipitated from the drying solution droplets without any pre-existing lipid templates or structures. The detailed formation process of the rugose lipid particle structure remains unclear at this point. In addition to the temperature-dependent mobility of lipid molecules that has been investigated, other factors such as the interactions between DSPC and $CaCl_2$, and the distribution of different lipid phases in the feedstock might also be important. For instance, emulsion-based spray drying has been used for the manufacture of the highly porous PulmoSphere™ / Aerosphere® DSPC particles despite the outlet temperature's being higher than the lipid main phase transition temperature (40, 67, 68). This discrepancy may be related to the use of placeholder agents like PFOB to provide pore-forming

templates as well as to a high-pressure homogenization process to facilitate incorporation of calcium ions during feedstock preparation, the latter which has been proven to increase the lipid phase transition temperature and prevent the particles from sintering at elevated temperatures (36, 44). Nonetheless, for the suspension-based spray drying method developed in this study, the need to keep spray drying outlet temperatures below the main phase transition temperature of the lipid proved critical to the manufacture of rugose lipid particles. Despite the small batch size and short production time used in this study, the high production yield numbers recorded in **Table IV** demonstrate the promising nature of the rugose lipid particle system with respect to manufacturability.

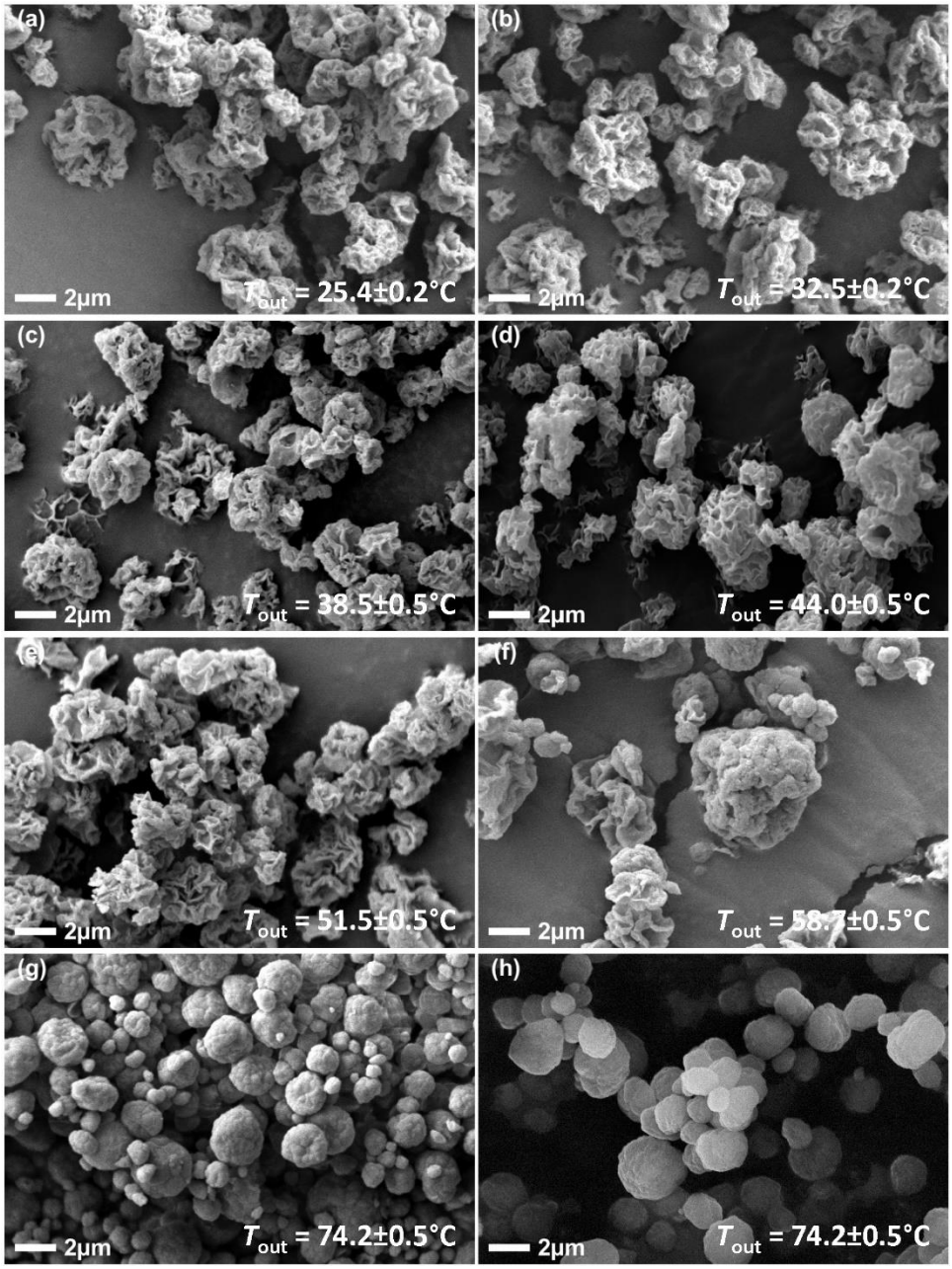

Fig. 6 Micrographs of particles from spray dried batch #2 (a, RLP-55T_f-35T_{in}), #3 (b, RLP-55T_f-45T_{in}), #4 (c, RLP-55T_f-55T_{in}), #5(d, RLP-55T_f-65T_{in}), #6 (e, RLP-55T_f-75T_{in}), #7 (f, RLP-55T_f-90T_{in}), and #8 (g, RLP-55T_f-120T_{in}) show the dependence of particle morphology on spray drying outlet temperature. Particles

from batch #8 (h) sampled in-line using a single-nozzle impactor prior to cyclone collection show morphology similar to that of particles collected by the cyclone.

Dispersibility and aerosol performance

Lipid particles spray dried from the control batch (#6, RLP-55T_f-75T_{in}) were selected for *in vitro* aerosol performance testing. In addition, since all the batches with a spray drying outlet temperature lower than the lipid main phase transition temperature showed similarly rugose particle surfaces as presented in **Fig. 6**, particles from one additional batch (#4, RLP-55T_f-55T_{in}) with a relatively lower rugosity were also tested for dispersibility for comparison purposes. The primary particle size distribution for particles from batch #4 was also measured in-process and the results plotted in **Fig. 4** together with those of the control case. With a similar feedstock preparation process, the same feedstock concentration, and the same initial droplet size, particles from the two batches showed very similar particle size distributions as expected and were all in the respirable range. Moisture content measurement by Karl Fischer titration (C30, Mettler Toledo, OH, USA) showed that both powders after spray drying and more than 24 h vacuum drying had similarly low moisture contents: 1.66 ± 0.10% for batch #4 and 1.51 ± 0.03% for batch #6.

Particle size distributions of the lung dose measured *in vitro* are shown in **Fig. 7** and were used as the input for the regional lung deposition modeling. As the *in vitro* aerosol performance characterization and regional lung deposition modeling results listed in **Table V** show, high emitted doses and total lung doses were achieved for both batches. About 86% and 93% of loaded powders were emptied from the capsules, respectively, which is promising for dry powder inhaler applications. The extrathoracic depositions were similar for both samples at ~37%. More than 50% total lung dose was also achieved for both batches. In comparison, the control batch performed slightly better than batch #4. However, even with the lower particle rugosity for the particles from batch #4, the powder still performed very well, meaning that the rugose particle surface is very effective in improving powder dispersibility (63, 69), with the improvement plateauing at higher rugosities. Considering that the total lung dose of commercially available dry powder inhalers typically ranges from 5 to 40% (70-72), the achieved numbers show substantial improvement and great potential for DPI applications. The regional deposition results indicated that, despite being tested with a low-resistance DPI device at a low pressure drop (~3.4kPa) and a high flow rate (100 LPM), about 60% of the emitted dose bypassed the extrathoracic region and entered the lung; meanwhile, 70% of the total lung dose penetrated into the deep lung with only about 30% deposited in the tracheobronchial region, showing excellent powder dispersibility and deep lung penetration capability for the tested rugose lipid particles. Higher emitted dose, lower tracheobronchial deposition, and higher alveolar deposition would be expected if a more efficient DPI device were used and the powders tested at a lower flow rate (72).

The achieved aerosol performance is even comparable to that of the PulmoSphere™ powder formulation, which also mainly consists of DSPC lipid and $CaCl_2$. It has been reported that compared to traditional DPI formulations, PulmoSphere™-based porous particle dry powder formulations enable highly efficient delivery to the lungs, with a high total lung dose ranging from 40% to 70% (36, 37). The only porous particle-based commercial dry powder inhaler, Tobi® Podhaler® has been reported to have a high emitted dose of –0 - 95% and a total lung dose of –5 - 60% (73). Despite being not as porous, the rugose lipid particles prepared in this study using the newly developed method provided excellent aerosol performance. This is mainly because the porous particles usually have many more internal pores than open pores, and sometimes the porous particles even have relatively smooth surfaces (41). The internal

pores, however, are not essential for drug loading, especially when used in carrier-based formulations. Therefore, the highly rugose lipid particles developed in this study might not be as porous as the PulmoSphere™ particles, which can easily have specific surface areas above 20 m^2/g (36), but their more rugose particle surfaces and more numerous open cavities can potentially lead to comparable dispersibility and drug loading capacity (39).

Table V *In vitro* aerosol performance characterization and regional deposition modeling results for two of the selected lipid particle batches: #4 (RLP-55T_f-55T_{in}) and #6 (RLP-55T_f-75T_{in})

Lot		**RLP-55T_f-55T_{in}**	**RLP-55T_f-75T_{in}**
Batch		4	6
Moisture content (%)		1.66±0.01	1.51±0.03
Emitted dose / loaded dose in capsule (%)		86.4 ± 4.4	92.8 ± 2.5
Fraction of Emitted Dose	Extrathoracic deposition (%)	36.6 ± 7.3	36.8 ± 2.4
	Tracheobronchial deposition (%)	18.6 ± 1.5	19.9 ± 0.4
	Alveolar deposition (%)	44.7 ± 6.9	43.3 ± 2.0
Total lung dose / loaded dose in capsule (%)		54.4 ± 5.0	58.6 ± 1.5
Fraction of Lung Dose	Tracheobronchial deposition (%)	29.6 ± 3.4	31.5 ± 0.6
	Alveolar deposition (%)	70.4 ± 3.4	68.5 ± 0.6

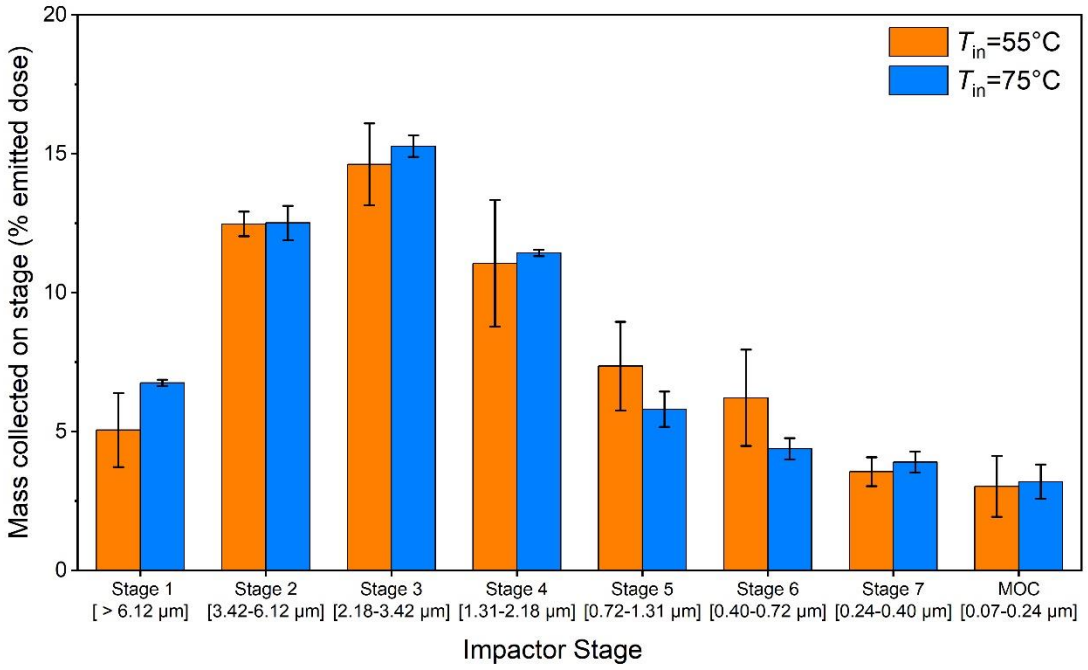

Fig. 7 Particle size distributions measured downstream of the Alberta Idealized Throat for two of the selected lipid particle batches: #4 (RLP-55T_f-55T_{in}) and #6 (RLP-55T_f-75T_{in}), expressed as the mass fraction of emitted dose. Error bars denote standard deviation.

Application to longer-chain lipids

The temperature requirements in the spray drying process to produce highly rugose DSPC lipid particles have been shown to be directly linked to the specific main phase transition temperature of DSPC at 55 °C, which is considered relatively low and less desirable from a manufacturing point of view. At a lower outlet temperature, the relative humidity at the outlet of the dryer increases for the same vapor mass fraction in the exhaust drying gas. The feed rate therefore needs to be reduced, or the gas flow rate increased, to keep the moisture content in the powder manageable. The latter approach runs into limitations because the droplet residence time in the dryer decreases, and the particles may not dry completely at the lower evaporation rate because of the lower inlet temperature. To avoid this potential problem, one would need a larger dryer body, which is not available in benchtop spray dryers. Hence, development would need to occur on mid-scale dryers, which are more costly and may cause issues with later commercial scale-up. It is therefore desirable to replicate the spray drying of such highly rugose lipid particles at higher outlet temperatures.

Longer-chain PC lipids with higher main phase transition temperatures, i.e., DAPC and 22:0 PC, were spray dried using the same approach while meeting the requirements for the feedstock preparation temperature and dryer outlet temperature in relation to their T_m. Rugose particles of the longer-chain lipids with morphologies similar to those of the DSPC particles were obtained as predicted and are shown in **Fig. 8**. While the DSPC particles spray dried with a dryer outlet temperature at 58.7 °C (batch #7) all exhibited a diminishment of their rugose surface features, both the DAPC and 22:0 PC lipids presented here retained their rugose structures at even higher T_{out}. This result further verifies the earlier finding that it is not the absolute spray drying outlet temperature that affects the final particle morphology but instead the relation between the outlet temperature and the main phase transition temperature of the lipid.

The rugosity values of 4.0 and 3.0 for these two batches (#10 and #11) were comparable to those for the DSPC particles spray dried at relatively lower temperatures (batches #2-4), one of which (batch #4) also demonstrated excellent aerosol performance. The successful application of the newly developed method for the spray drying of longer-chain lipids DAPC and 22:0 PC shows the potential of using similar processing conditions for the manufacture of other PC lipids and even lipids of different classes for, but not limited to, respirable drug delivery applications. Higher temperatures used for the manufacture of these DAPC and 22:0 PC particles can be advantageous in actual batch production because of the resulting improved manufacturability and potentially higher throughput.

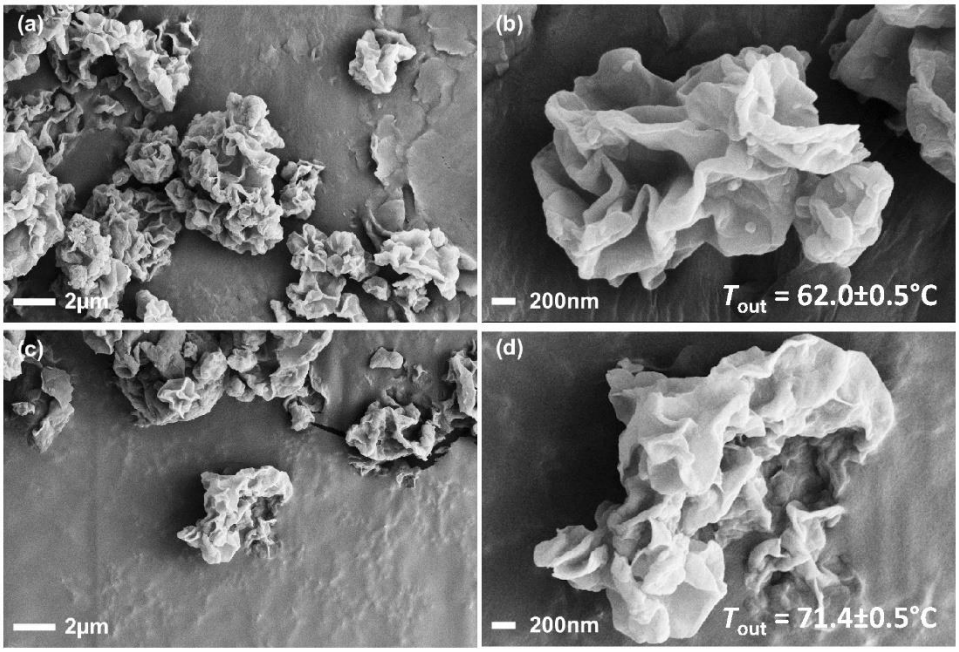

Fig. 8 Highly rugose long-chain lipid particles of (a-b) DAPC (#10, RLP-65T_f-95T_{in}) and (c-d) 22:0 PC (#11, RLP-75T_f-110T_{in}) spray dried using the newly developed method.

CONCLUSIONS

As non-toxic excipients endogenous to the lungs, lipids such as DSPC have attributes favorable to their use in formulation platforms for delivering active pharmaceutical ingredients to the lung. This study introduced a novel spray drying method that produces highly rugose lipid particles. Processing conditions including the feedstock preparation temperature, spray drying outlet temperature, and their direct relation to the main phase transition temperature of the spray dried lipid were identified as critical in producing and maintaining highly rugose surface features and can be optimized to achieve large specific surface area for good dispersibility and potentially higher drug loading capacity. *In vitro* aerosol performance characterization and regional lung deposition results show that these rugose lipid particles outperform most commercially available DPI formulations in terms of dispersibility and deep lung penetration, presenting a promising formulation approach for respiratory drug delivery applications. The rugose lipid particle platform presented here features a feedstock preparation process that dispenses with the use of any pore-forming agents or high-pressure homogenization steps. This is the first time such highly rugose lipid particles within the respirable range have been directly spray dried from an aqueous suspension-based feedstock with a simplified feedstock preparation process. Not limited to the tested DSPC lipid, this new method has been demonstrated to be applicable to longer-chain PC lipids (DAPC and 22:0 PC) and potentially to lipids of different classes for the efficient manufacture of rugose lipid particles for various applications. The processing conditions could potentially be further optimized to maximize the specific surface area and rugosity for each different lipid, and storage stability under various conditions needs to be established. Applications of the new drug loading platform in other areas, such as pressurized metered-dose inhalers and stabilization of biologics, require further exploration.

DECLARATION

Funding Statement

This work was supported by the Natural Sciences and Engineering Research Council of Canada through its Collaborative Research & Development program (Grant CRDPJ 543336-19).

Conflicts of Interest Statement

The authors declare no conflict of interest.

Acknowledgments and Disclosures

The authors acknowledge language editing provided by Luba Slabyj. PC, KL, NC, DLB are employees of AstraZeneca and may own stock or stock options.

REFERENCES

1. Patton JS, Byron PR. Inhaling medicines: delivering drugs to the body through the lungs. Nat Rev Drug Discov. 2007;6(1):67-74. http://dx.doi.org/10.1038/nrd2153
2. Sanders M. Inhalation therapy: an historical review. Prim Care Respir J. 2007;16(2):71-81. https://doi.org/10.3132/pcrj.2007.00017
3. Ibrahim M, Verma R, Garcia-Contreras L. Inhalation drug delivery devices: technology update. Med Devices (Auckl). 2015;8:131. http://dx.doi.org/10.2147/MDER.S48888
4. Le Brun P, De Boer A, Frijlink H, Heijerman H. A review of the technical aspects of drug nebulization. Pharm World Sci. 2000;22(3):75-81. https://doi.org/10.1023/A:1008786600530
5. Myrdal PB, Sheth P, Stein SW. Advances in metered dose inhaler technology: formulation development. AAPS PharmSciTech. 2014;15(2):434-455. http://dx.doi.org/10.1208/s12249-013-0063-x
6. Stein SW, Sheth P, Hodson PD, Myrdal PB. Advances in metered dose inhaler technology: hardware development. AAPS PharmSciTech. 2014;15(2):326-338. http://dx.doi.org/10.1208/s12249-013-0062-y
7. Chougule MB, Padhi BK, Jinturkar KA, Misra A. Development of dry powder inhalers. Recent Pat Drug Deliv Formul. 2007;1(1):11-21. https://doi.org/10.2174/187221107779814159
8. Frijlink H, De Boer A. Dry powder inhalers for pulmonary drug delivery. Expert Opin Drug Deliv. 2004;1(1):67-86. http://dx.doi.org/10.1517/17425247.1.1.67
9. de Boer AH, Hagedoorn P, Hoppentocht M, Buttini F, Grasmeijer F, Frijlink HW. Dry powder inhalation: past, present and future. Expert Opin Drug Deliv. 2017;14(4):499-512. http://dx.doi.org/10.1080/17425247.2016.1224846
10. Chan JGY, Wong J, Zhou QT, Leung SSY, Chan H-K. Advances in device and formulation technologies for pulmonary drug delivery. AAPS PharmSciTech. 2014;15(4):882-897. https://doi.org/10.1208/s12249-014-0114-y
11. Telko MJ, Hickey AJ. Dry powder inhaler formulation. Respir Care. 2005;50(9):1209-1227.
12. Weers JG, Miller DP. Formulation design of dry powders for inhalation. J Pharm Sci. 2015;104(10):3259-3288. https://doi.org/10.1002/jps.24574
13. Vehring R. Pharmaceutical particle engineering via spray drying. Pharm Res. 2008;25(5):999-1022. https://dx.doi.org/10.1007/s11095-007-9475-1
14. Pilcer G, Amighi K. Formulation strategy and use of excipients in pulmonary drug delivery. Int J Pharm. 2010;392(1-2):1-19. https://doi.org/10.1016/j.ijpharm.2010.03.017
15. Hamishehkar H, Rahimpour Y, Javadzadeh Y. The role of carrier in dry powder inhaler. In: Sezer AD, editor. Recent Advances in Novel Drug Carrier Systems. Rijeka, Croatia: InTech; 2012. p. 39-66. http://dx.doi.org/10.5772/51209

16. Zillen D, Beugeling M, Hinrichs WL, Frijlink HW, Grasmeijer F. Natural and bioinspired excipients for dry powder inhalation formulations. Curr Opin Colloid Interface Sci. 2021:101497. https://doi.org/10.1016/j.cocis.2021.101497
17. Fröhlich E, Salar-Behzadi S. Oral inhalation for delivery of proteins and peptides to the lungs. Eur J Pharm Biopharm. 2021;163:198-211. https://doi.org/10.1016/j.ejpb.2021.04.003
18. Pilcer G, Wauthoz N, Amighi K. Lactose characteristics and the generation of the aerosol. Adv Drug Del Rev. 2012;64(3):233-256. http://dx.doi.org/10.1016/j.addr.2011.05.003
19. Chang RYK, Chow MY, Khanal D, Chen D, Chan H-K. Dry powder pharmaceutical biologics for inhalation therapy. Adv Drug Del Rev. 2021. https://doi.org/10.1016/j.addr.2021.02.017
20. Ngan CL, Asmawi AA. Lipid-based pulmonary delivery system: a review and future considerations of formulation strategies and limitations. Drug Deliv Transl Res. 2018;8(5):1527-1544. https://doi.org/10.1007/s13346-018-0550-4
21. Li J, Wang X, Zhang T, Wang C, Huang Z, Luo X, Deng Y. A review on phospholipids and their main applications in drug delivery systems. Asian J Pharm Sci. 2015;10(2):81-98. https://dx.doi.org/10.1016/j.ajps.2014.09.004
22. Cipolla D, Shekunov B, Blanchard J, Hickey A. Lipid-based carriers for pulmonary products: preclinical development and case studies in humans. Adv Drug Del Rev. 2014;75:53-80. https://dx.doi.org/10.1016/j.addr.2014.05.001
23. Scalia S, Young PM, Traini D. Solid lipid microparticles as an approach to drug delivery. Expert Opin Drug Deliv. 2015;12(4):583-599. https://doi.org/10.1517/17425247.2015.980812
24. Jaspart S, Piel G, Delattre L, Evrard B. Solid lipid microparticles: formulation, preparation, characterisation, drug release and applications. Expert Opin Drug Deliv. 2005;2(1):75-87. https://doi.org/10.1517/17425247.2.1.75
25. Vanbever R, Mintzes JD, Wang J, Nice J, Chen D, Batycky R, Langer R, Edwards DA. Formulation and physical characterization of large porous particles for inhalation. Pharm Res. 1999;16(11):1735-1742. https://doi.org/10.1023/A:1018910200420
26. Bosquillon C, Lombry C, Preat V, Vanbever R. Influence of formulation excipients and physical characteristics of inhalation dry powders on their aerosolization performance. J Control Release. 2001;70(3):329-339. https://doi.org/10.1016/S0168-3659(00)00362-X
27. Minne A, Boireau H, Horta MJ, Vanbever R. Optimization of the aerosolization properties of an inhalation dry powder based on selection of excipients. Eur J Pharm Biopharm. 2008;70(3):839-844. https://doi.org/10.1016/j.ejpb.2008.06.013
28. Pilcer G, Sebti T, Amighi K. Formulation and characterization of lipid-coated tobramycin particles for dry powder inhalation. Pharm Res. 2006;23(5):931-940. https://doi.org/10.1007/s11095-006-9789-4
29. Eleftheriadis GK, Akrivou M, Bouropoulos N, Tsibouklis J, Vizirianakis IS, Fatouros DG. Polymer–Lipid microparticles for pulmonary delivery. Langmuir. 2018;34(11):3438-3448. https://doi.org/10.1021/acs.langmuir.7b03645
30. Shetty N, Hou J, Yanez E, Shur J, Cheng J, Sun CC, Nagapudi K, Narang AS. Effect of lipidic excipients on the particle properties and aerosol performance of high drug load spray dried particles for inhalation. J Pharm Sci. 2021. https://doi.org/10.1016/j.xphs.2021.09.004
31. Jaspart S, Bertholet P, Piel G, Dogné J-M, Delattre L, Evrard B. Solid lipid microparticles as a sustained release system for pulmonary drug delivery. Eur J Pharm Biopharm. 2007;65(1):47-56. https://doi.org/10.1016/j.ejpb.2006.07.006
32. Scalia S, Salama R, Young P, Traini D. Preparation and in vitro evaluation of salbutamol-loaded lipid microparticles for sustained release pulmonary therapy. J Microencapsul. 2012;29(3):225-233. https://doi.org/10.3109/02652048.2011.646326

33. Mezzena M, Scalia S, Young PM, Traini D. Solid lipid budesonide microparticles for controlled release inhalation therapy. AAPS J. 2009;11(4):771-778. http://dx.doi.org/10.1208/s12248-009-9148-6
34. Scalia S, Haghi M, Losi V, Trotta V, Young PM, Traini D. Quercetin solid lipid microparticles: a flavonoid for inhalation lung delivery. Eur J Pharm Sci. 2013;49(2):278-285. http://dx.doi.org/10.1016/j.ejps.2013.03.009
35. Maretti E, Rossi T, Bondi M, Croce MA, Hanuskova M, Leo E, Sacchetti F, Iannuccelli V. Inhaled Solid Lipid Microparticles to target alveolar macrophages for tuberculosis. Int J Pharm. 2014;462(1-2):74-82. http://dx.doi.org/10.1016/j.ijpharm.2013.12.034
36. Weers J, Tarara T. The PulmoSphere™ platform for pulmonary drug delivery. Ther Deliv. 2014;5(3):277-295. https://dx.doi.org/10.4155/tde.14.3
37. Weers JG, Miller DP, Tarara TE. Spray-Dried PulmoSphere™ Formulations for Inhalation Comprising Crystalline Drug Particles. AAPS PharmSciTech. 2019;20(3). http://dx.doi.org/10.1208/s12249-018-1280-0
38. Geller DE, Weers J, Heuerding S. Development of an inhaled dry-powder formulation of tobramycin using PulmoSphere™ technology. J Aerosol Med Pulm Drug Deliv. 2011;24(4):175-182. https://doi.org/10.1089/jamp.2010.0855
39. Miller DP, Tan T, Tarara TE, Nakamura J, Malcolmson RJ, Weers JG. Physical characterization of tobramycin inhalation powder: I. rational design of a stable engineered-particle formulation for delivery to the lungs. Mol Pharm. 2015;12(8):2582-2593. https://doi.org/10.1021/acs.molpharmaceut.5b00147
40. Tarara TE, Hartman MS, Gill H, Kennedy AA, Weers JG. Characterization of suspension-based metered dose inhaler formulations composed of spray-dried budesonide microcrystals dispersed in HFA-134a. Pharm Res. 2004;21(9):1607-1614. https://doi.org/10.1023/B:PHAM.0000041455.13980.f1
41. Vehring R, Lechuga-Ballesteros D, Joshi V, Noga B, Dwivedi SK. Cosuspensions of microcrystals and engineered microparticles for uniform and efficient delivery of respiratory therapeutics from pressurized metered dose inhalers. Langmuir. 2012;28(42):15015-15023. https://dx.doi.org/10.1021/la302281n
42. Fisher AB. Lung lipid composition and surfactant biology. In: Parent RA, editor. Comparative biology of the normal lung: Academic Press; 2015. p. 423-466. https://doi.org/10.1016/B978-0-12-404577-4.00022-9.
43. Praphawatvet T, Peters JI, Williams III RO. Inhaled nanoparticles - an updated review. Int J Pharm. 2020:119671. https://doi.org/10.1016/j.ijpharm.2020.119671
44. D'Sa D, Williams L, Speck J, Dwivedi S, Lechuga D. Thermodynamic and Structural effects of CaCl2 on the Phase Transitions and Structures of Distearoyl-Phosphatidylcholine (DSPC) by Differential Scanning Calorimetry and X-Ray Diffraction. In.AAPS Annual Meeting and Exposition. Washington, DC, US; 2011.
45. Corzo C, Fuchsbichler A, Savencu I, Urich JA, Zimmer A, Lochmann D, Reyer S, Salar-Behzadi S. Lipid-microparticles for pulmonary delivery of active pharmaceutical ingredients: impact of lipid crystallization on spray-drying processability. Int J Pharm. 2021:121259. https://doi.org/10.1016/j.ijpharm.2021.121259
46. Koynova R, Caffrey M. Phases and phase transitions of the phosphatidylcholines. Biochimica et Biophysica Acta (BBA)-Reviews on Biomembranes. 1998;1376(1):91-145. https://doi.org/10.1016/S0304-4157(98)00006-9
47. Marsh D. Handbook of lipid bilayers, 2nd Edition: CRC press; 2013. https://dx.doi.org/10.1201/b11712

48. Janiak MJ, Small DM, Shipley GG. Temperature and compositional dependence of the structure of hydrated dimyristoyl lecithin. J Biol Chem. 1979;254(13):6068-6078. https://doi.org/10.1016/S0021-9258(18)50520-2
49. Marsh D. General features of phospholipid phase transitions. Chem Phys Lipids. 1991;57(2):109-120. https://doi.org/10.1016/0009-3084(91)90071-I
50. Szoka Jr F, Papahadjopoulos D. Comparative properties and methods of preparation of lipid vesicles (liposomes). Annu Rev Biophys Bioeng. 1980;9(1):467-508. https://doi.org/10.1146/annurev.bb.09.060180.002343
51. Ivey J. Particle formation from evaporating microdroplets for inhaled drug delivery. In.Mechanical Engineering. Edmonton, Alberta: University of Alberta; 2018. https://doi.org/10.7939/R3RB6WJ3S
52. Hoe S, Ivey JW, Boraey MA, Shamsaddini-Shahrbabak A, Javaheri E, Matinkhoo S, Finlay WH, Vehring R. Use of a fundamental approach to spray-drying formulation design to facilitate the development of multi-component dry powder aerosols for respiratory drug delivery. Pharm Res. 2014;31(2):449-465. https://dx.doi.org/10.1007/s11095-013-1174-5
53. Carrigy NB, Liang L, Wang H, Kariuki S, Nagel TE, Connerton IF, Vehring R. Trileucine and pullulan improve anti-Campylobacter bacteriophage stability in engineered spray-dried microparticles. Ann Biomed Eng. 2019. https://doi.org/10.1007/s10439-019-02435-6
54. Wang H, Bhambri P, Ivey J, Vehring R. Design and pharmaceutical applications of a low-flow-rate single-nozzle impactor. Int J Pharm. 2017;533(1):14-25. http://dx.doi.org/10.1016/j.ijpharm.2017.09.047
55. Rouquerol F, Rouquerol J, Sing KS, Llewellyn P, Maurin G. Adsorption by powders and porous solids: principles, methodology and applications: Academic press; 2014. http://dx.doi.org/10.1016/B978-0-08-097035-6.00007-3
56. Carrigy NB, Ordoubadi M, Liu Y, Melhem O, Barona D, Wang H, Milburn L, Ruzycki CA, Finlay WH, Vehring R. Amorphous pullulan trehalose microparticle platform for respiratory delivery. Int J Pharm. 2019;563:156-168. https://doi.org/10.1016/j.ijpharm.2019.04.004
57. Pharmacopeia US. <601> Aerosols, nasal sprays, metered dose inhalers, and dry powder inhalers. In.US Pharmacopeial Convention, Rockville, MD, USA; 2012.
58. Javaheri E, Shemirani FM, Pichelin M, Katz IM, Caillibotte G, Vehring R, Finlay WH. Deposition modeling of hygroscopic saline aerosols in the human respiratory tract: Comparison between air and helium–oxygen as carrier gases. J Aerosol Sci. 2013;64:81-93. http://dx.doi.org/10.1016/j.jaerosci.2013.04.010
59. Ruzycki CA, Murphy B, Nathoo H, Finlay WH, Martin AR. Combined in Vitro-in Silico Approach to Predict Deposition and Pharmacokinetics of Budesonide Dry Powder Inhalers. Pharm Res. 2020;37(10):1-19. https://doi.org/10.1007/s11095-020-02924-7
60. Tavernini S, Farina DJ, Martin AR, Finlay WH. Using Filters to Estimate Regional Lung Deposition with Dry Powder Inhalers. Pharm Res. 2021;38(9):1601-1613. https://doi.org/10.1007/s11095-021-03082-0
61. Vierros S, Sammalkorpi M. Phosphatidylcholine reverse micelles on the wrong track in molecular dynamics simulations of phospholipids in an organic solvent. J Chem Phys. 2015;142(9):094902. https://doi.org/10.1063/1.4914022
62. Pichot R, Watson RL, Norton IT. Phospholipids at the interface: current trends and challenges. Int J Mol Sci. 2013;14(6):11767-11794. https://doi.org/10.3390/ijms140611767
63. Wang H, Nobes DS, Vehring R. Particle surface roughness improves colloidal stability of pressurized pharmaceutical suspensions. Pharm Res. 2019;36(3):43. https://dx.doi.org/10.1007/s11095-019-2572-0

64. Baldelli A, Vehring R. Analysis of cohesion forces between monodisperse microparticles with rough surfaces. Colloids Surf Physicochem Eng Aspects. 2016;506:179-189. http://dx.doi.org/10.1016/j.colsurfa.2016.06.009
65. Vehring R, Foss WR, Lechuga-Ballesteros D. Particle formation in spray drying. J Aerosol Sci. 2007;38(7):728-746. https://dx.doi.org/10.1016/j.jaerosci.2007.04.005
66. Wang H, Tan P, Barona D, Li G, Hoe S, Lechuga-Ballesteros D, Nobes DS, Vehring R. Characterization of the suspension stability of pharmaceuticals using a shadowgraphic imaging method. Int J Pharm. 2018;548(1):128-138. http://dx.doi.org/10.1016/j.ijpharm.2018.06.053
67. Dellamary LA, Tarara TE, Smith DJ, Woelk CH, Adractas A, Costello ML, Gill H, Weers JG. Hollow porous particles in metered dose inhalers. Pharm Res. 2000;17(2):168-174. http://dx.doi.org/10.1023/A:1007513213292
68. Lechuga-Ballesteros D, Vehring R, Dwivedi S. A new co-suspension MDI platform: scientific foundations of mono, dual and triple combination products. In.Respiratory Drug Delivery Europe; 2011. p. 101-112.
69. Adi S, Adi H, Chan H-K, Tong Z, Yang R, Yu A. Effects of mechanical impaction on aerosol performance of particles with different surface roughness. Powder Technol. 2013;236:164-170. https://dx.doi.org/10.1016/j.powtec.2012.02.051
70. Newman S, Busse W. Evolution of dry powder inhaler design, formulation, and performance. Respir Med. 2002;96(5):293-304. https://dx.doi.org/10.1053/rmed.2001.1276
71. Borgström L, Olsson B, Thorsson L. Degree of throat deposition can explain the variability in lung deposition of inhaled drugs. J Aerosol Med. 2006;19(4):473-483. https://doi.org/10.1089/jam.2006.19.473
72. Clark AR, Weers JG, Dhand R. The confusing world of dry powder inhalers: It is all about inspiratory pressures, not inspiratory flow rates. J Aerosol Med Pulm Drug Deliv. 2020;33(1):1-11. https://doi.org/10.1089/jamp.2019.1556
73. Ung KT, Chan H-K. Effects of ramp-up of inspired airflow on in vitro aerosol dose delivery performance for certain dry powder inhalers. Eur J Pharm Sci. 2016;84:46-54. http://dx.doi.org/10.1016/j.ejps.2016.01.005